Rydberg-atom trajectories in a ponderomotive optical lattice

Kelly Cooper Younge[1], Sarah Elizabeth Anderson and Georg Raithel

FOCUS Center, Department of Physics, University of Michigan, Ann Arbor, MI 48109, USA
E-mail: kyounge@umich.edu

Abstract. Using semiclassical simulations, we investigate the trajectories and the microwave spectra of Rydberg atoms excited in a ponderomotive optical lattice. We relate distinct features found in the microwave spectra to characteristic types of trajectory. Several methods are presented that are designed to greatly improve the trapping efficiency of the lattice and to generalize the trapping from one to three dimensions.

Contents

[1] Author to whom any correspondence should be addressed.

1. Introduction

The advent of laser cooling and quantum information science has brought about renewed interest in Rydberg-atom physics. Cooling atoms with laser beams enables the preparation of samples of Rydberg atoms that interact with each other over long periods of time within small regions of space (early references include [1]–[3]). Coherent Rydberg-atom interactions present possible venues for quantum information processing [4, 5]. Quantum gates based on a Rydberg excitation blockade have been demonstrated recently [6, 7].

Rydberg-atom traps present an opportunity for new directions in this research area. Extensions of the work in [6, 7] will necessitate sequential gate operations repeatedly utilizing the same atoms. As a means of avoiding motional decoherence, a Rydberg-atom trapping device will probably be required. Further applications of Rydberg-atom traps may also arise in high-resolution spectroscopy. Long-lived, trapped Rydberg atoms could be used for measurements of fundamental constants, particularly the Rydberg constant, and quantum defects, and for field sensing (see, for instance, [8]). Additional opportunities for trapped Rydberg-atom spectroscopy may arise in sensing local fields and forces near surfaces, such as atom chips (for a recent example, see [9]). Rydberg-atom traps could generally become useful for research involving dense, cold gases of Rydberg atoms, as well as for research involving the formation of cold Rydberg atoms via recombination in ultracold plasmas (for recent reviews, see [10, 11]). Nonlinear optical effects such as super-radiance [12] and electromagnetically induced transparency [13] would possibly be enhanced if Rydberg atoms were trapped at periodic lattice sites.

Rydberg atoms have been experimentally trapped for the first time in a high-field Ioffe–Pritchard atom trap that provides a field strength of about 3 T at the trap minimum [14, 15]. An electrostatic Rydberg-atom trap based on the Stark effect has been realized by Merkt and co-workers [16, 17]. Trapping Rydberg atoms in inhomogeneous magnetic fields has been studied theoretically in great detail by Schmelcher and co-workers (see, for instance, [18]). While static-field devices such as those employed and proposed in [14]–[18] serve the purpose of trapping Rydberg atoms in a well-defined region of space, they induce substantial inhomogeneous level shifts due to the static fields applied to the atoms. For applications in spectroscopy and quantum information processing, it will be beneficial to develop a trapping method that causes minimal trap-induced level shifts while still providing trapping functionality. Promising candidates for atom traps exhibiting small trap-induced level shifts are optical lattices. Optical lattices are periodic light-shift potentials that result from the interaction of atoms with the electric field of multiple interfering laser beams [19, 20]. They are widely employed for localizing cold atoms at periodic sites. A universal type of optical lattice for Rydberg atoms can be created utilizing the ponderomotive energy of quasi-free Rydberg electrons in rapidly oscillating optical fields [21]. The main difference between Rydberg-atom optical lattices and lattices for ground-state atoms lies in the size of the atoms relative to the lattice period. Ground-state atoms can be considered point-like relative to the lattice period, while Rydberg atoms typically have a size similar to that of the lattice period. The relatively large Rydberg-atom size enables novel methods for spectroscopy. For instance, electro-optic modulation of the lattice beams has been proposed as a powerful method for driving coherent, site-selective, high-order multipole transitions between Rydberg levels [22].

In recent work on such applications, we have studied Rydberg atoms in ponderomotive optical lattices with depths of the order of tens of MHz [23]. Cold ^{85}Rb Rydberg

atoms were prepared by two-step laser excitation in a magneto-optical trap (MOT; atom temperature $\sim$200 μK). In the crossed-beam excitation region, the lower-transition ($5S_{1/2} \rightarrow 5P_{3/2}$, wavelength 780 nm) beam had a full-width at half-maximum (FWHM) of the intensity profile of 150 μm and the upper-transition ($5P_{3/2} \rightarrow nS_{1/2}$, principal quantum number n, wavelength $\approx$480 nm) beam of 25 μm. The optical lattice was created by a retro-reflected 1064 nm laser beam (power $\sim$1 W) focused to a FWHM of 13 μm. The lattice focus was carefully overlapped with the crossed-beam Rydberg-excitation region. Under the excitation conditions used, all Rydberg atoms that were excited were located at an intensity maximum of the optical lattice. The Rydberg-atom trapping potential in the lattice was then probed using microwave spectroscopy. The measurements allowed us to verify the effectiveness of the lattice as a trapping device and to estimate the fraction of trapped atoms. A detailed discussion of this experiment can be found in [23].

In this paper, we first discuss a fruitful analogy between the problem of a Rydberg atom in an optical lattice and that of a simple plane pendulum. Several qualitatively different classes of trajectory are identified. We then analyze the microwave spectra obtained in [23] in terms of the underlying center-of-mass trajectories of the Rydberg atoms in the optical lattice. Using a semiclassical simulation, certain types of trajectory can be associated with the features observed in the microwave spectra. We then discuss several strategies that will lead to greatly improved Rydberg-atom trapping.

2. Classical phase-space dynamics of Rydberg atoms in a one-dimensional ponderomotive lattice

Due to the vast difference between typical Rydberg-atom Kepler frequencies ($\sim$10^{11} Hz) and optical frequencies ($\gtrsim$10^{14} Hz), the dominant effect of a non-resonant laser field applied to a Rydberg atom is that the field adds a ponderomotive term, $e^2 E^2 / 4 m_e \omega^2$, to the usual atomic potential in the Rydberg electron's Hamiltonian. Here, $-$e is the electron charge and m_e its mass, ω the angular frequency of the field and E the electric-field amplitude. If the field consists of two counter-propagating laser beams, the spatial period of the intensity modulation in the resultant standing wave is $\lambda/2$, where $\lambda = 2\pi c/\omega$. If the period is much larger than the atom, the ponderomotive term does not vary substantially over the atom's volume. For laser beams with equal linear polarization and field amplitude E_0, the trapping potential acting on the Rydberg atom's center-of-mass coordinate then approximately equals the free-electron ponderomotive potential in the lattice,

$$U(Z) = \frac{V_0}{2} \left(1 - \cos\left(2kZ\right)\right), \tag{1}$$

where $k = 2\pi/\lambda$, Z is the atom's center-of-mass coordinate in the lattice-beam direction and V_0 is the maximum potential depth, $V_0 = e^2 E_0^2 / m_e \omega^2$. The equation of motion for the atom is

$$\ddot{Z} = -\frac{V_0 k}{m} \sin(2kZ). \tag{2}$$

In comparison, the equation of motion for a plane pendulum is

$$\ddot{\theta} = -\frac{g}{L} \sin\theta. \tag{3}$$

From equations (2) and (3), it is obvious that there is a direct analogy between the motion of an atom in the optical lattice under consideration and the well-known angular dynamics of a
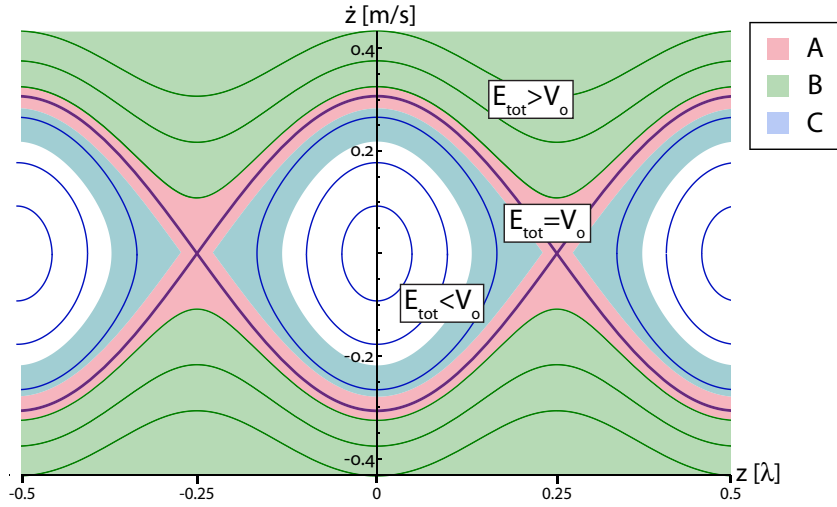
Figure 1. Phase-space diagram for motion of atoms in a ponderomotive optical lattice. The different shaded regions correspond to the trajectory classes A, B and C seen in figure 2.

plane pendulum. This analogy can be used to gain some insight. In both cases, for energies less than the potential depth the trajectories are trapped (bound) and periodic, with small-amplitude oscillation frequencies of $\sqrt{2V_0k^2/m}$ and $\sqrt{g/L}$, respectively. As the energy approaches the potential depth, the oscillation amplitude increases and the frequency decreases. When the energy equals the potential depth, the oscillation period diverges and the trajectory includes a fixed point. The fixed point corresponds to the atom or the pendulum resting in an unstable equilibrium at the respective potential maximum. For higher energies, the motion is periodic but unbound.

Figure 1 shows the phase-space diagram reflecting this dynamics. To be specific, we consider ^{85}Rb atoms in a lattice with $V_0 = 10$ MHz, lattice laser wavelength $\lambda = 1064$ nm and total energy E_{tot}. Following equation (1), the equation of motion can be written as

$$\dot{Z} = \sqrt{\frac{V_0}{m}\left(\cos\left(2kZ\right) - 1\right) + \frac{2E_{tot}}{m}}. \tag{4}$$

The phase-space diagram has a separatrix at an energy that equals the lattice depth ($E_{tot} = V_0$; bold line in figure 1). For $E_{tot} < V_0$, the phase-space trajectories are periodic and resemble closed ellipses, corresponding to atoms that are trapped inside one lattice well. For $E_{tot} > V_0$, the phase trajectories are periodic but not closed, corresponding to untrapped atoms running over the lattice wells. The separatrix forms the boundary between the two cases; it has hyperbolic fixed points at the lattice potential maxima, $\{(z = (n+1/2)\lambda/2, \dot{z} = 0), n \in \mathbb{Z}\}$. Trajectories close to the separatrix have a long period, and atoms on such trajectories spend most of their time in the vicinity of the hyperbolic fixed points.

In the experiment described in [23], the depth V_0 was derived from laser-spectroscopic lineshift measurements of optical Rydberg-excitation lines. Typical values of V_0 were of the order of 10 MHz, corresponding to small-amplitude oscillation periods of about 3.5 μs. Further, atoms had thermal kinetic energies of about 2 MHz and were excited into Rydberg states near the lattice intensity maxima. Hence, the lattice depth was much larger than the kinetic

energy, and the relevant phase-space trajectories were mostly concentrated near the separatrix, as indicated in figure 1. As a result, both trapped and untrapped classes of trajectory were excited in [23]. The different classes of trajectory correspond to well-defined features in the measured microwave spectra. This will be discussed in the following section.

3. Microwave spectra of Rydberg transitions in an optical lattice

In the analysis presented in the previous section, it was assumed that the Rydberg atom is much smaller than the lattice period, resulting in a potential depth $V_0 = e^2 E_0^2 / m_e \omega^2$. This approximation becomes inaccurate for principal quantum numbers large enough that the Rydberg wavefunction extends over a significant portion of a lattice well. In that case, the adiabatic lattice potential of the Rydberg atom follows from [24]:

$$V_{ad}(\mathbf{R}) = \int d^3 r \, V_p(\mathbf{r} + \mathbf{R}) \, |\psi(\mathbf{r})|^2, \tag{5}$$

where $\mathbf{R}$ is the center-of-mass coordinate of the atom, $\mathbf{r}$ is the relative coordinate of the Rydberg electron, $V_p(\mathbf{r} + \mathbf{R})$ is the position-dependent free-electron ponderomotive potential, $\frac{e^2 |\mathbf{E}(\mathbf{r}+\mathbf{R})|^2}{4m_e \omega^2}$, and $\psi(\mathbf{r})$ is the Rydberg wavefunction. As a result, the adiabatic trapping potentials depend on the atomic state. Typically, with increasing principal quantum number, n, the adiabatic Rydberg-atom trapping potentials, $V_{ad}(\mathbf{R})$, become shallower than the underlying free-electron potential, $V_p(\mathbf{R})$, and may even become inverted for certain aspect ratios of atom size and lattice period. Generally, angular quantum numbers also affect the detailed shape of $V_{ad}(\mathbf{R})$. The adiabatic potentials are, in general, complicated and accompanied by substantial lattice-induced state mixing [24]. However, the potentials for nS Rydberg atoms are fairly simple due to the non-degeneracy of these states (hence, no state mixing) and the isotropy of their wavefunctions. In the one-dimensional (1D) lattice considered here, the adiabatic potentials of nS Rydberg states are still of the general form of equation (1); the state dependence primarily affects the potential depth. While the state dependence of V_{ad} will, in most cases, not affect the functionality of the lattice as a trapping device for Rydberg atoms, it leads to frequency shifts of transitions between different Rydberg states. In [23], this lattice-induced frequency shift and its state dependence have been used to verify the effectiveness of the ponderomotive optical lattice.

Figure 2 shows a microwave spectrum, taken from [23], of the 50S → 51S transition for atoms in a Rydberg-atom lattice having a modulation depth of 10 MHz. Atoms were excited into the 50S Rydberg state near a lattice potential maximum. Atoms that have very little initial kinetic energy spend a majority of their time near a hyperbolic fixed point in figure 1. In the plane pendulum analogy, this case corresponds to an inverted pendulum near an unstable equilibrium. Calculating the shift of the 50S → 51S microwave transition using equation (5) for an atom resting at a hyperbolic fixed point, we obtain line shifts of ∼ −430 MHz. We therefore expect that the pink region in figure 1 should correspond to peak A in figure 2. Atoms that are trapped oscillate in a single lattice well. Since for a Rydberg atom localized at a potential minimum we calculate a ∼ +430 MHz shift, for trapped Rydberg atoms we expect upshifted microwave transition frequencies. Hence, trapped Rydberg atoms should contribute to region C in the microwave spectrum (light blue phase-space area in figure 1). Finally, for atoms that have enough energy to traverse many lattice wells during the given atom–field interaction time, one might expect that positive and negative lineshifts mostly average out. As those atoms move somewhat slower near the potential maxima, where the lineshift is negative, we expect a
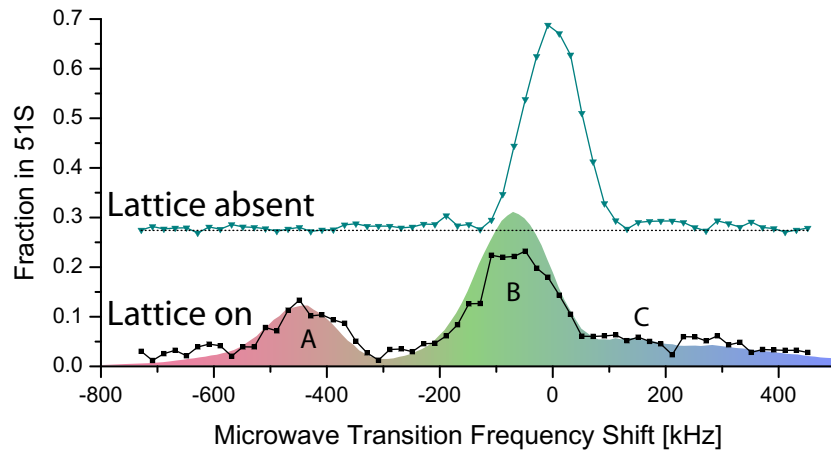
Figure 2. Experimental microwave spectra (dots and thin lines) of the 50S $\rightarrow$ 51S transition outside of the lattice (offset vertically for clarity) and for a Rydberg lattice modulation depth of $V_0 = 10$ MHz. The shaded curve shows the result of a simulation. The coloring of the shaded curve corresponds to the coloring of the different regions of figure 1.

relatively small, negative, net shift. Thus, atoms running across wells are expected to generate peak B in figure 2 (light green phase-space area in figure 1).

4. Trajectory simulations

In order to prove the scenario laid out in the previous paragraph and to gain more insight into the behavior of Rydberg atoms in an optical lattice, we have performed numerical simulations of the Rydberg-atom dynamics. The internal-state dynamics is treated quantum mechanically, whereas the center-of-mass coordinate, **R**, is treated classically. While a quantum treatment of the center-of-mass motion would be fairly straightforward [19, 20], the numerically less intensive classical treatment is entirely sufficient because of the large depth of the Rydberg-atom lattices. In the present work, the lattice depth amounts to thousands of recoil energies, rendering center-of-mass quantization effects and tunneling irrelevant.

In the classical treatment of the center-of-mass dynamics, we begin with assuming a Boltzmann distribution of ground-state atom positions and velocities in the dipole-trap potential the optical lattice generates for the 5S ground-state atoms. For the temperature in the optical dipole-trap potential, we use 200μK, following an estimate in [23]. After randomly selecting positions and momenta following this Boltzmann distribution, we determine the probabilities that the atoms are excited into the 50S Rydberg level as follows. Since the optical lattice generates an attractive, red-shifted dipole-trap potential for ground-state atoms while it generates a repulsive, blue-shifted ponderomotive lattice for the Rydberg atoms, the optical Rydberg excitation frequency is a strong function of position. According to the experiment in [23], we assume that the optical Rydberg excitation is resonant at the lattice-field maxima, which is where the ground-state atoms collect, and that the net optical excitation bandwidth is 5 MHz (based on estimates of laser linewidths and Rydberg level broadening due to stray electric and magnetic fields). For each 50S Rydberg atom produced, its classical center-of-mass

trajectory, $\mathbf{R}(t)$, is computed using a Runge–Kutta method. This is done using the adiabatic ponderomotive lattice potential $V_{ad,50S}(\mathbf{R})$, calculated via equation (5). For each realization, the integration time is randomly chosen between 6 and 8 μs, in agreement with the experiment.

To simulate microwave spectra like that shown in figure 2, the microwave-driven quantum evolution operator, $\hat{U}$, is integrated along the classical center-of-mass trajectory, $\mathbf{R}(t)$, which is known from the procedure explained in the previous paragraph. The adiabatic lattice potentials $V_{ad,50S}(\mathbf{R})$ and $V_{ad,51S}(\mathbf{R})$ govern both the classical center-of-mass trajectory and, via the lattice-induced level shifts, the microwave-driven quantum dynamics between the coupled Rydberg levels. For a given $\mathbf{R}(t)$, the quantum evolution operator in the internal state space $\{|50S\rangle, |51S\rangle\}$ follows from $i\hbar(\partial/\partial t)\hat{U} = \hat{H}\hat{U}$, with a Hamiltonian

$$\hat{H}(t) = \begin{pmatrix} V_{ad,50S}(\mathbf{R})(t) & \hbar\chi \\ \hbar\chi & V_{ad,51S}(\mathbf{R})(t) \end{pmatrix}. \tag{6}$$

The constant value of the real two-photon microwave Rabi frequency, χ, is chosen such that the simulated final 51S-population without lattice approximately matches the value of 40% observed in the experiment (top curve in figure 2). To obtain satisfactory statistics, the procedure is repeated until the simulated sample contains 10 000 realizations of the Rydberg-atom evolution. After performing the simulation for a set of microwave detunings, we obtain simulated microwave spectra by plotting the average final 51S population versus the microwave detuning. The Rabi frequency of the microwave transition is adjusted to yield good agreement between on-resonant experimental and simulated 51S probabilities without lattice. Experimental and simulated spectra are compared in figure 2.

To visualize the types of trajectory that, at a given microwave detuning, contribute the most to the observed microwave spectrum, we identify the subset $S_{0.01}$ of 1% of all simulated Rydberg-atom trajectories that result in the highest microwave transition probabilities. In figure 3, we plot the $S_{0.01}$-subsets of Rydberg-atom trajectories for three values of microwave detunings intended to correspond to features A, B and C observed in the 50S $\rightarrow$ 51S microwave spectrum. Parameters selected for this simulation are tailored to match the experimental parameters used to measure the data shown in figure 2.

Figure 3(a) shows the $S_{0.01}$-subset of trajectories at a -430 kHz shift of the 50S $\rightarrow$ 51S transition, i.e. the frequency shift at which the A-signal is observed in figure 2. This frequency offset is equal to the -430 kHz frequency shift of the 50S $\rightarrow$ 51S transition that an atom frozen at a lattice maximum (hyperbolic fixed point in figure 1) would experience. Inspecting the histogram in the top panel of figure 3, it is seen that the $S_{0.01}$-subset of trajectories at -430 kHz indeed spends a vast majority of their time near lattice maxima, while only occasionally sampling other parts of the lattice. These atoms have total energies in the range of V_0 and correspond to the pink region in the phase-space map in figure 1. The simulation hence confirms that the A-component of the microwave spectrum in figure 2 corresponds to atoms on trajectories that do not deviate much from the lattice maxima.

Figure 2(b) shows the $S_{0.01}$-subset of trajectories that give rise to a -80 kHz shift, corresponding to the B-peak in the microwave spectrum. There is a striking difference between the trajectories seen in panels (a) and (b): atoms with trajectories shown in panel (b) have enough energy after excitation to roam over many lattice wells during the given interaction time. Inspecting the histogram in the middle panel of figure 3, it is seen that those atoms spend only a little more time in regions where the lattice-induced shift of the 50S $\rightarrow$ 51S transition is negative (lattice maxima) than they do in regions where the shift is positive (lattice minima).

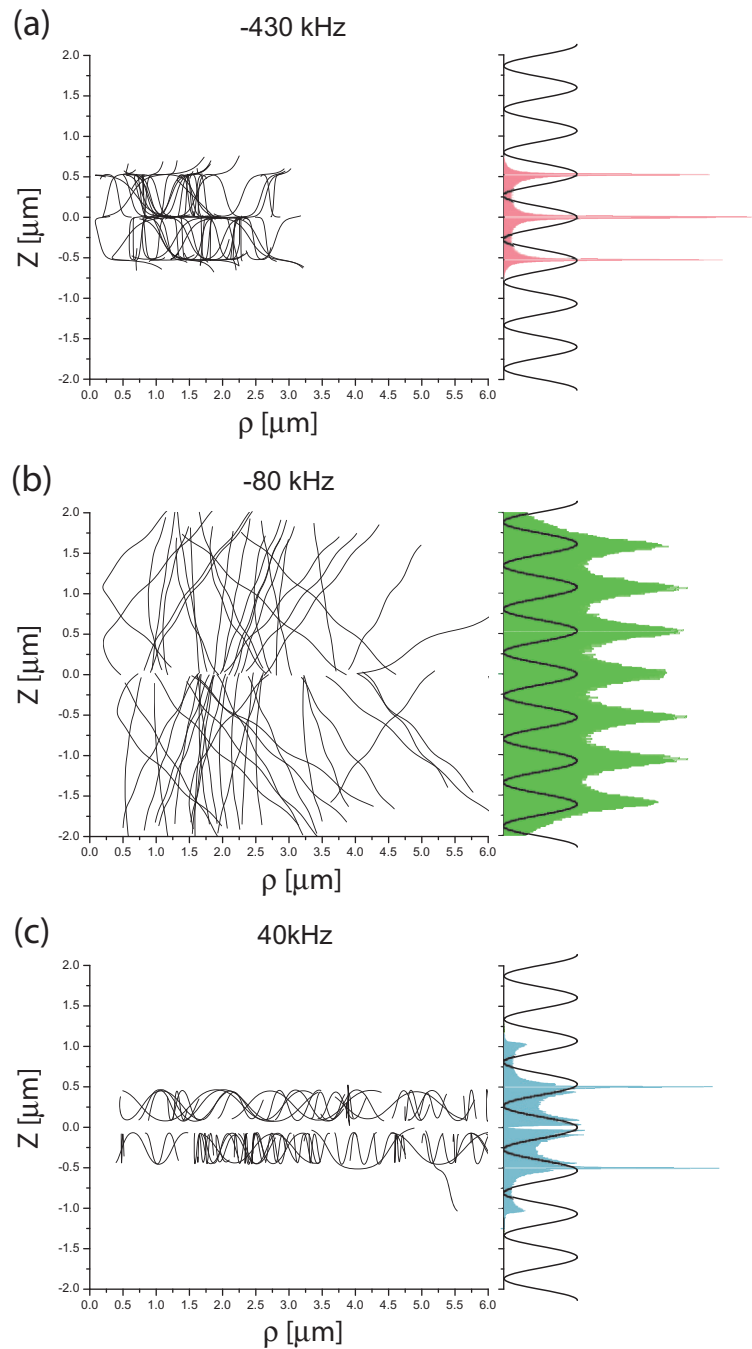**IOP** Institute of Physics **Φ** DEUTSCHE PHYSIKALISCHE GESELLSCHAFT

Figure 3. Calculated $S_{0.01}$-subsets of Rydberg-atom trajectories in a ponderomotive optical lattice for the same parameters as in figure 2 and for the indicated values of the microwave detuning (-430, -80 and $40\,$kHz from top to bottom). The histograms on the right show the corresponding probability distributions along the Z-coordinate.

Hence, on average there is only a small net negative shift, in agreement with the B-peak in figure 2. The simulation, hence, confirms that the B-component of the microwave spectrum is due to atoms sampling many lattice wells, corresponding to the green area in the phase-space

map in figure 1. The simulations further show that when exciting the Rydberg atoms near the maxima of the ponderomotive lattice, the majority of trajectories are in the green phase-space area in figure 1.

Panel (c) shows a typical $S_{0.01}$-subset of trajectories that result in a +40 kHz blue shift of the 50S → 51S transition (i.e. in between the B- and the C-signatures of the microwave spectrum in figure 2). Most of these trajectories are confined to a single lattice unit cell. Hence, these atoms are trapped in a single well and cannot freely roam through the lattice. During the given atom–field interaction time (6–8 μs), the atoms have enough time to undergo two or three oscillations in the lattice well in which they are trapped.

In figure 3, we have (intentionally) shown $S_{0.01}$-subsets of trajectories for values of the microwave detuning at which these subsets have quite uniform, distinctive characteristics. At a detuning of −430 kHz, the $S_{0.01}$-subset mostly consists of atoms spending most of their time near hyperbolic fixed points in figure 1, at −80 kHz it mostly consists of atoms running across many lattice wells and at +40 kHz it mostly consists of trapped atoms. We note that for other detunings the $S_{0.01}$-subsets of trajectories are not, in general, uniform in their qualitative characteristics. For example, in the detuning range $\gtrsim 100$ kHz, both trapped trajectories as in panel (c) and untrapped ones as in panel (b) contribute. Noting that the microwave excitation probability depends on both the Fourier spectrum of the microwave pulse as well as the time dependence of the microwave detuning imposed by the atoms' motion through the lattice, it is not very surprising that there are microwave detunings for which several distinct types of trajectory contribute to the $S_{0.01}$-subsets.

5. Rydberg-atom trapping

The fraction of atoms that are confined to a single lattice well depends strongly on the experimental parameters used to generate the lattice potential and on the optical Rydberg-excitation frequency. In the case studied in [23], the fact that ground-state atoms were excited into Rydberg states at a potential maximum of the lattice provided the Rydberg atoms with near-maximal initial potential energy. In this case, the only atoms that were trapped were those that were fortuitously both excited slightly displaced from a lattice maxima due to the linewidth of the excitation laser and also had little kinetic energy. Some of these atoms did not have enough energy to climb over lattice potentials and were trapped. From the spectra shown in figure 2 and the calculated trajectories in figure 3, we estimate that about 5% of all excited Rydberg atoms were trapped in the lattice over the 8 μs atom–field interaction time.

Atoms trapped in a 1D ponderomotive lattice will still leave the lattice transversely because the lattice potential is repulsive in the directions transverse to the axis of the lattice laser beams. For the lattice used in [23], atoms with a temperature of 200 μK excited on the lattice axis leave the lattice region within about 20 μs.

For these reasons, there are two factors that need to be addressed in order to improve the trapping functionality of ponderomotive optical lattices. Firstly, instead of exciting Rydberg atoms at lattice maxima, with near-maximal potential energy, a method needs to be found to initially prepare the Rydberg atoms in a lattice minimum. Secondly, the lattice-beam geometry needs to be re-designed to enable transverse trapping, resulting in a 3D optical Rydberg-atom trap. In the following paragraphs, we present methods to address both of these issues.

IOP Institute of Physics ⏀ DEUTSCHE PHYSIKALISCHE GESELLSCHAFT

5.1. Improvement of longitudinal trapping performance

Since the lattice acts as a red-detuned optical dipole trap for the laser-cooled ground-state atoms, the ground-state atoms collect at the maxima of the lattice laser field. In [23], the ground-state and Rydberg-state level shifts in the optical lattice were employed to selectively excite ground-state atoms trapped in the optical dipole trap into Rydberg states. As a result, the Rydberg atoms were excited at locations of high potential energy in the ponderomotive Rydberg-atom trapping potential. This resulted in a low fraction of Rydberg atoms that were trapped at all, and the temperature of the trapped atoms was high.

One method to increase the number of trapped atoms would be to use a blue-detuned trap, as this type of trap would have the potential minima for the ground and Rydberg states in the same location. However, in this arrangement the atoms would be attracted to minima in the laser field intensity. Therefore, to retain the atoms in the trap, it would be necessary to manipulate the beam to create a 'donut' shape, with a dark volume surrounded by blue-detuned light. This beam shape is less straightforward to generate and poses difficulties for loading ground-state atoms into the trap. In addition, a shorter wavelength trap would come at the expense of a smaller depth in the ponderomotive potential, which would have to be compensated for by an increase in laser power. As a simpler alternative to demonstrate higher-efficiency Rydberg-atom trapping as well as lower trapped-atom temperatures, in the following we discuss a method that involves a phase shift of a red-detuned lattice.

A π phase shift applied to one of the lattice laser beams immediately after Rydberg excitation can serve to translate the location of the lattice potential maxima by $\lambda/4$. Immediately after the translation, atoms that are initially excited at the potential maxima will find themselves at a potential minimum. Hence, they will be efficiently trapped in the 1D ponderomotive Rydberg-atom lattice. The lattice phase shift can be accomplished through a number of means, for example with a voltage-controlled waveplate. For the method to work, it is essential that the phase shift be applied over a time interval that is much shorter than the round-trip period of the atoms in the lattice wells.

Microwave spectroscopy is a powerful method to probe the effectiveness of the lattice translation. To show this, we have simulated microwave spectra like the one shown in figure 2 as a function of an instantaneous translation of the lattice after Rydberg excitation. Figure 4 shows the simulated microwave spectra as a function of lattice translation. The optical Rydberg-atom excitation is assumed to be resonant at the lattice field maxima prior to the translation. A translation of $\lambda/4$ corresponds to the case where the lattice is completely inverted immediately after excitation (i.e. all atoms excited at lattice maxima are instantaneously transferred to lattice minima). Figure 4 shows that, as the translation is increased from zero, the microwave spectrum undergoes an overall blue frequency shift, which is suggestive of more trapped atoms. For a translation of $\lambda/4$, the microwave spectrum exclusively consists of a blue-shifted peak centered at +380 kHz. This value approaches the frequency shift of +430 kHz that an atom pinned down at a ponderomotive-lattice minimum would experience. Figure 4, hence, indicates that microwave spectroscopy is suited to prove the enhanced trapping performance and that for a translation of $\lambda/4$ most Rydberg atoms should be longitudinally trapped.

Figure 5 shows the trajectories of Rydberg atoms in a lattice with varying amounts of lattice translation. The parameters used to calculate these trajectories are tailored to match the experimental parameters used to measure the data in figure 2. In contrast to figure 3, in figure 5 we do not selectively plot trajectories that maximize the microwave transition probability at
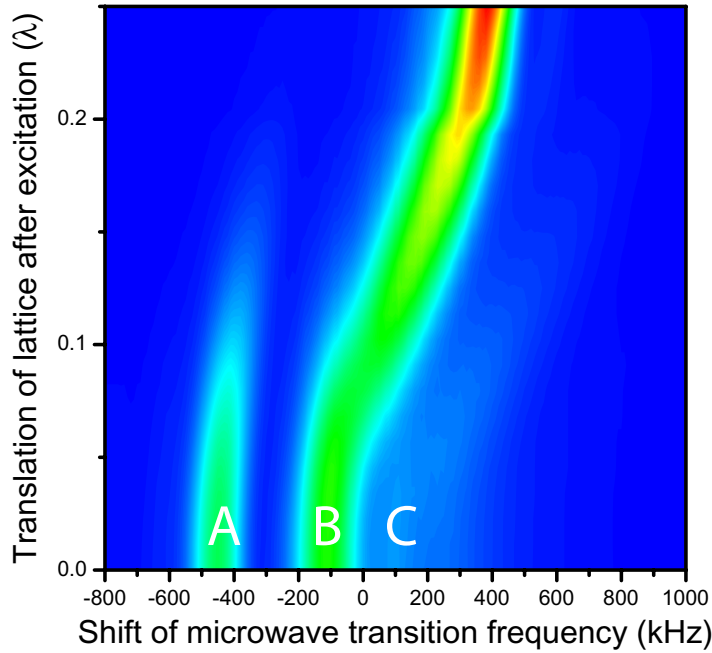
Figure 4. Contour plot of microwave spectra of the 50S → 51S transition as a function of microwave detuning and lattice translation after excitation.

a specific microwave frequency—we rather show trajectories of random samples of Rydberg atoms optically excited in the lattice. On the right side of figure 5, we display histograms of the Z-positions of the atoms in the lattice. Without a lattice translation, most atoms roam over many wells within the lattice. They slow down near the lattice maxima, thus giving rise to peaks in the histogram at these points. Upon closer inspection, one finds that a small percentage of the atoms are trapped, as discussed in sections 3 and 4. If the lattice is translated by $\lambda/8$ (atoms moved to lattice inflection points after excitation), a great majority of the atoms become trapped. These atoms exhibit a sloshing motion between classical turning points in a single lattice well. The sloshing motion leads to a pair of peaks in the Z-probability distribution. Lastly, a $\lambda/4$ translation (atoms moved to lattice minima after excitation) leads to trapping of essentially all excited Rydberg atoms. These atoms are also tightly confined within a single lattice site, and will remain trapped until they exit the lattice transversely. The temperature of the trapped Rydberg atoms is similar to that of the ground-state atoms prior to excitation.

5.2. Three-dimensional trapping

As the ponderomotive lattice generally produces light forces pointing away from the light-field maxima, it is less straightforward to generate 3D ponderomotive traps than it is to generate attractive (red-detuned) optical dipole traps. In the following, we describe an efficient method to generate a 3D ponderomotive Rydberg-atom trap using only two Gaussian beams.

A typical optical lattice formed with a pair of identical laser beams has an electric field of the approximate form

$$\sqrt{\frac{2P}{\pi w(Z)}}e^{-\rho^2/w(Z)^2}[e^{ikZ+ik\rho^2/2R(Z)-iG(Z)} + e^{-ikZ-ik\rho^2/2R(Z)+iG(Z)}], \tag{7}$$
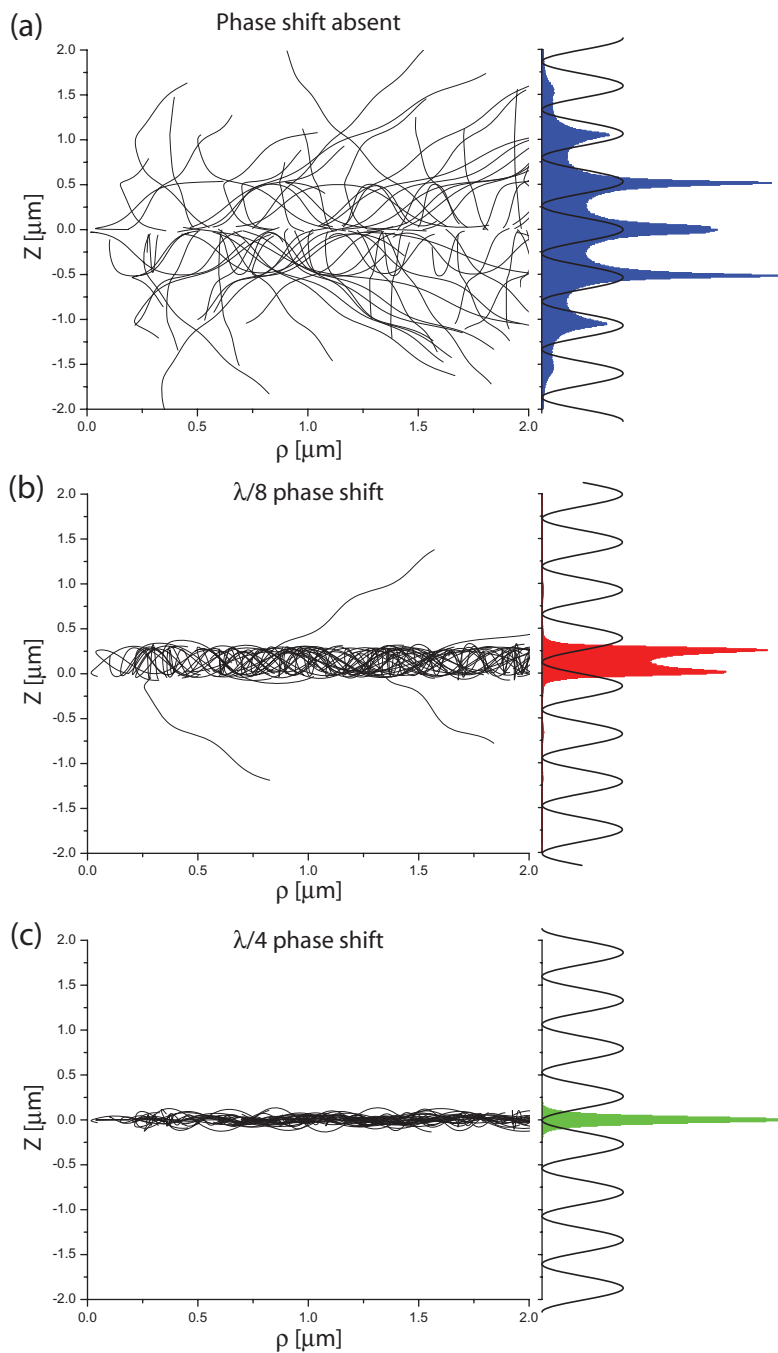
Figure 5. Rydberg-atom trajectories for the indicated amounts of lattice shift after excitation. The right side of each graph contains a histogram of Z-positions in the lattice. The sine waves overlapping the histograms show the locations of the lattice maxima and minima relative to the trajectories and the histograms.

where P is the total power in each beam, ρ the distance from the axis of the beams, $w(Z)$ the beam waist, Z the coordinate along the beam axis, $R(Z)$ a parameter representing the wavefront curvature, and $G(Z)$ the Guoy phase. A transverse lattice potential gradient can be formed either
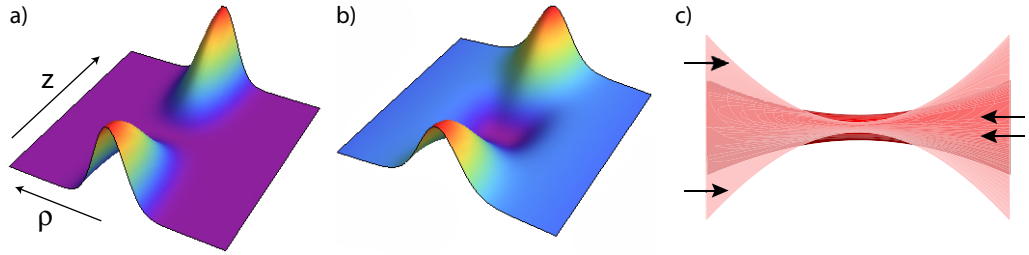
Figure 6. 3D intensity profiles for a two-beam optical lattice with equal beam sizes (a) and for beams with a spot size ratio of 10 : 1 (b). The peak intensities of both beams are equal. (c) A beam diagram.

by offsetting the focus of one of the laser beams from the other or by adjusting the radial beam size of one of the beams. In any case, it is straightforward to realize conditions such that, at the location of the atoms, one beam is larger in diameter than the other. In that case, the electric field is given by

$$\sqrt{\frac{2P_1}{\pi w_1(Z)}} e^{-\rho^2/w_1(Z)^2} e^{ikZ} + \sqrt{\frac{2P_2}{\pi w_2(Z)}} e^{-\rho^2/w_2(Z)^2} e^{-ikZ}. \tag{8}$$

Here, $w_1(Z)$ and $w_2(Z)$ are the different beam-waist functions of the beams. The wavefront curvature and the Guoy phase terms, as shown in equation (6), were found to be insignificant in the parameter range of interest, and are left out in equation (7) for simplicity.

The 3D intensity profile of a standard optical lattice compared to a lattice where one beam is a factor of ten larger than the other is shown in figures 6(a) and (b). The beam powers are chosen such that the square-root factors in equation (7) are equal for both beams. In figure 6(b), one can see that a transverse force is generated that will confine cold atoms near the lattice axis. We refer to this as a 'bottle trap potential'. The transverse potential height is about one quarter that of the longitudinal barrier.

Figure 7 shows two typical trajectories of atoms trapped in a potential similar to that of figure 6(b). In the simulation, we have combined the bottle trap potential with a $\lambda/4$ phase shift of the lattice applied immediately after excitation. The same beam intensities as in figure 5 are used; however, one lattice beam has a FWHM of $1\,\mu$m, while the other beam has a FWHM of $10\,\mu$m. Atoms are now confined longitudinally and transversely. The trajectories radially oscillate back and forth between near $\rho = 0$ and the outer edge of the trap potential near $\rho \approx 1\,\mu$m. The apparent repulsion near $\rho = 0$ is a result of the centrifugal barrier, $L_Z^2/(2m\rho^2)$, which occurs in the 3D calculation. (The calculation in figure 1 was 1D; hence there was no centrifugal term).

6. Conclusion

We have used semiclassical simulations to model the dynamics of Rydberg atoms in a ponderomotive optical lattice. The simulations have allowed us to interpret the microwave spectra obtained in [23] in terms of different types of center-of-mass trajectories that occur in the lattice. We have then shown in the simulations that a lattice shift can be used to improve the trapping efficiency of the lattice to nearly 100%. Further, modified beam geometries were
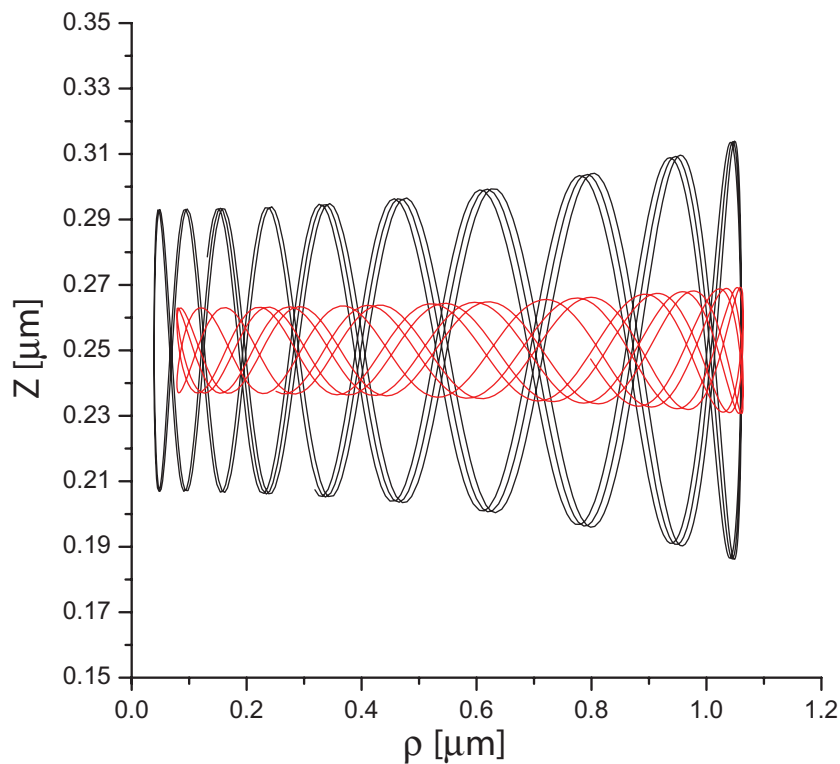
IOP Institute of Physics   **Φ** DEUTSCHE PHYSIKALISCHE GESELLSCHAFT

Figure 7. Two example trajectories of atoms in a potential as shown in figure 6(b). Both atoms are three-dimensionally trapped.

shown to be a viable tool to allow 3D Rydberg-atom trapping in ponderomotive optical lattices. Experiments for improving trapping using lattice phase shifts as well as efforts to demonstrate 3D trapping are in progress.

Acknowledgments

References

[1] Anderson W R, Veale J R and Gallagher T F 1998 *Phys. Rev. Lett.* **80** 249–52
[2] Mourachko I, Comparat D, De Tomasi F, Fioretti A, Nosbaum P, Akulin V M and Pillet P 1998 *Phys. Rev. Lett.* **80** 253–6
[3] Dutta S K, Feldbaum D, Walz-Flannigan A, Guest J R and Raithel G 2001 *Phys. Rev. Lett.* **86** 3993–6
[4] Jaksch D, Cirac J I, Zoller P, Rolston S L, Côté R and Lukin M D 2000 *Phys. Rev. Lett.* **85** 2208
[5] Lukin M D, Fleischhauer M, Côté R, Duan L M, Jaksch D, Cirac J I and Zoller P 2001 *Phys. Rev. Lett.* **87** 037901
[6] Isenhower L, Urban E, Zhang X L, Gill A T, Johnson T A, Walker T G and Saffman M 2010 *Phys. Rev. Lett.* **104** 010503

[7] Wilk T, Gaetan A, Evellin C, Wolters J, Miroshnychenko Y, Grangier P and Browaeys A 2010 *Phys. Rev. Lett.* **104** 010502

[8] Jentschura U D, Mohr P J and Tan J N 2010 *J. Phys.* B **43** 074002

[9] Tauschinsky A, Thijssen R M T, Whitlock S, van Linden van den Heuvell H B and Spreeuw R J C 2010 *Phys. Rev. A* **81** 063411

[10] Killian T C, Pattard T, Pohl T and Rost J M 2007 *Phys. Rep.* **449** 77–130

[11] Pohl T, Sadeghpour H R and Schmelcher P 2009 *Phys. Rep.* **484** 181–229

[12] Moi L, Goy P, Gross M, Raimond J M, Fabre C and Haroche S 1983 *Phys. Rev. A* **27** 2043–64

[13] Mohapatra A K, Jackson T R and Adams C S 2007 *Phys. Rev. Lett.* **98** 113003

[14] Choi J-H, Guest J R, Povilus A P, Hansis E and Raithel G 2005 *Phys. Rev. Lett.* **95** 243001

[15] Choi J-H, Guest J R and Raithel G 2006 *Eur. Phys. J. D* **40** 19–26

[16] Vliegen E, Hogan S D, Schmutz H and Merkt F 2007 *Phys. Rev. A* **76** 023405

[17] Hogan S D and Merkt F 2008 *Phys. Rev. Lett.* **100** 043001

[18] Lesanovsky I and Schmelcher P 2005 *Phys. Rev. Lett.* **95** 053001

[19] Jessen P S and Deutsch I H 1996 *Adv. At. Mol. Phys.* **37** 95

[20] Morrow N V and Raithel G 2006 *Adv. At. Mol. Phys.* **53** 187

[21] Dutta S K, Guest J R, Feldbaum D, Walz-Flannigan A and Raithel G 2000 *Phys. Rev. Lett.* **85** 5551–4

[22] Knuffman B and Raithel G 2007 *Phys. Rev. A* **75** 053401

[23] Younge K C, Knuffman B, Anderson S E and Raithel G 2010 *Phys. Rev. Lett.* **104** 173001

[24] Younge K C, Anderson S E and Raithel G 2010 *New J. Phys.* **12** 023031